

Supersonic Flow over Annular Cavities at an Angle of Attack

S. V. Guvernyuk^a, M. M. Simonenko^{a,*}, and A. F. Zubkov^a

^aScientific Research Institute of Mechanics, Moscow State University, Moscow, 119192 Russia

*e-mail: sim1950@mail.ru

Received March 14, 2018; revised March 14, 2018; accepted March 14, 2018

Abstract—Results obtained for experimental studies on a supersonic flow over an axisymmetric cylindroconical body with an annular cavity of a rectangular axial cross section at an angle of attack and at Mach number $M = 2.5$ are presented. Data visualization of the flow structure, pressure measurements, and weight testing have been obtained for relative cavity lengths ranging from 6 to 18. The structure evolution and parameters of the flow over a cavity has been studied under a continuous change in the angle of attack in the range from -4° to 16° . Different flow modes corresponding to closed, open, and combined patterns of flow over a cavity have been identified. The existence ranges of aerodynamic hysteresis in the transition between flow modes from one pattern of flow over a cavity to another have been estimated in the space of dimensionless problem-determining parameters.

Keywords: annular cavity, supersonic flow, angle of attack, aerodynamic hysteresis

DOI: 10.1134/S0015462822601292

1. INTRODUCTION

Design features in the form of cavities (cavities, notches, cutouts, depressions) on the outer and inner surfaces of bodies are widely represented in the case of aerospace engineering objects. The purpose thereof is rather manifold, from solving the problems of stabilizing and increasing the range of supersonic jets (for example, when launching rockets from launch wind tunnels) to improving the quality of mixing fuel with an oxidizer, as well as stabilizing combustion in a supersonic flow and intensifying heat transfer. A special place is occupied by external annular cavities that as structural elements, occur in the structure of different objects of rocket and space engineering (carrier rockets, anti-aircraft missiles, artillery shells). In particular, external annular cavities can exert a stabilizing effect on flying axisymmetric bodies in a gaseous continuous medium.

Supersonic flow over cavities was studied experimentally [1–11] and numerically [4, 11–15]. The features of the supersonic flow over successively installed cavities [16, 17], as well as hypersonic flow over cavities [18] were considered. Different active and passive methods for controlling the flow in cavities have been studied [19–21]. Issues concerning the use of cavities for mixing fuel and oxidizer and for stabilizing combustion in a supersonic flow were studied [22, 23].

Despite a large number of experimental and numerical papers concerning the studies on supersonic flow over cavities, the understanding of flow physics within a cavity is still incomplete even in the simplest case of rectangular cavities. Typical experimental and numerical studies are devoted to the studies on supersonic flow over flat and annular cavities at a zero angle of attack. However, in real conditions, the flow around axisymmetric bodies usually occurs at an angle of attack, in which case the axial symmetry of the flow is violated and more complex three-dimensional flow structures are realized. The studies on the fundamental properties of a separated flow over cavities at an angle of attack is of great practical importance, too, both in choosing optimal patterns for flow around bodies with cavities, and in developing novel methods for controlling flows in a cavity.

This study is devoted to the results of experimental studies on a three-dimensional supersonic flow over an axisymmetric annular cavity having a rectangular cross section located on a cylindroconical body at an angle of attack. In the experiments, pressure has been measured inside the cavity, high-speed DVR shadow images have been registered for flow patterns, and weight testing models with cavities with different lengths has been performed under a continuous change in the angle of attack. The visualization results and weight measurements have been partially published in [9].

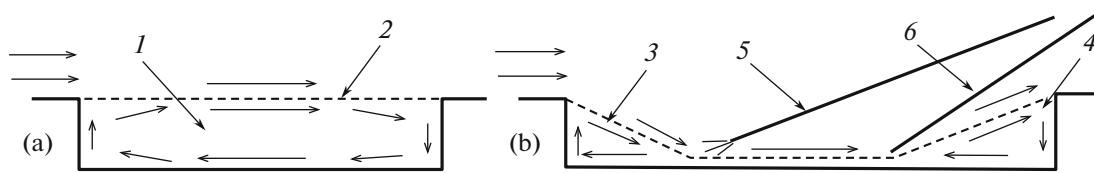


Fig. 1. Schematic diagram (a) for an open cavity and (b) for a closed cavity.

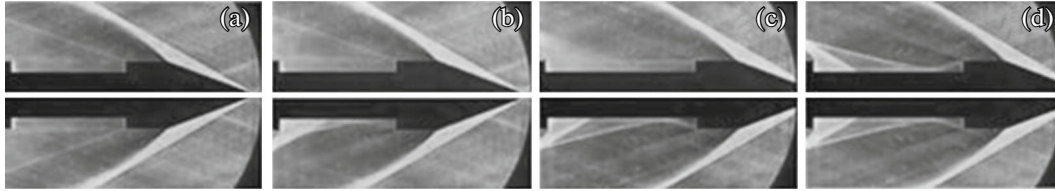


Fig. 2. The evolution of the structure of the supersonic flow over a cavity in the case of a continuous increase (top) and in the case of a continuous decrease (bottom) in λ : (a–d) $\lambda \approx 10.2, 10.3, 13.7, \text{ and } 13.8$.

2. THE FEATURES OF SUPERSONIC FLOW OVER CAVITIES

The supersonic flow over an annular cavity at a zero angle of attack is qualitatively similar to the flow over a flat cavity. The flow structure is determined primarily by a ratio between geometric dimensions, and depends on the condition of the boundary layer at the entrance to the cavity, as well as on Mach and Reynolds numbers. Within a cavity having a rectangular configuration, depending on the ratio between cavity length L and its depth h , two different flow patterns can be observed, as shown in Fig. 1 (flow is directed from the left to the right). If $\lambda = L/h$ is small ($\lambda < \lambda_o$), an open flow pattern is observed (open cavity). In this case, subsonic circulation flow 1 separated from the external supersonic flow by mixing layer 2 occurs inside the cavity. If λ exceeds a certain critical value ($\lambda > \lambda_c$), a closed flow pattern is observed (closed cavity). In this case, two isolated separation zones are formed in the cavity; zone 3 stays behind the front ledge, whereas zone 4 stays in front of the rear ledge.

In the supersonic flow field, compression and rarefaction waves, as well as shock waves occur: tail shock wave 5 behind the front separation zone, and shock wave 6 in front of the rear separation zone. The range of $\lambda_o < \lambda < \lambda_c$ corresponds to a so-called transition region, wherein both open and closed flow patterns can occur.

For the case of rectangular flat cavities and axisymmetric ones in a supersonic turbulent flow there are empirical estimates for the boundaries of the transition region: $\lambda_o = 9\text{--}10$, $\lambda_c = 13\text{--}14$. According to data obtained based on physical [8, 10] and numerical [14, 15] simulation, the transition region represents, in fact, a region of hysteresis in the cavity length. In the case of a continuous increase in length, the initially open cavity closed at $\lambda = \lambda_c$, whereas in the case of a continuous decrease in length, the closed cavity opened at $\lambda = \lambda_o$ (see Fig. 2 [8], the flow is directed from the right to the left).

The phenomenon of hysteresis is illustrated by a characteristic hysteresis loop on the graph plotted for the change in pressure P at the rear ledge of the cavity depending on λ (Fig. 3 [8]; the direction of change in λ on the corresponding branches of the graph is shown by arrows). Here and below, the value of pressure is related to the static pressure in the running-on flow.

With increasing λ in the case of an initially open cavity (curve 1), the pressure on the rear ledge monotonically increases. When $\lambda = \lambda_c$ is attained, the cavity becomes closed, and an abrupt increase in pressure is observed. With further decreasing pressure inside the closed cavity (curve 2), the pressure on the rear ledge does not decrease monotonically, which could be associated with a change in the position of the tail shock wave with respect to the shock wave in front of the separation at the rear ledge of the cavity and remains increased up to $\lambda = \lambda_o$. Then, at $\lambda = \lambda_o$, the cavity opens, which is accompanied by an abrupt decrease in pressure.

It has been experimentally established that at moderate Mach numbers ($M = 2.5\text{--}3.0$) the upper boundary of the hysteresis region, λ_c , is almost independent on the conditions of flow formation at the

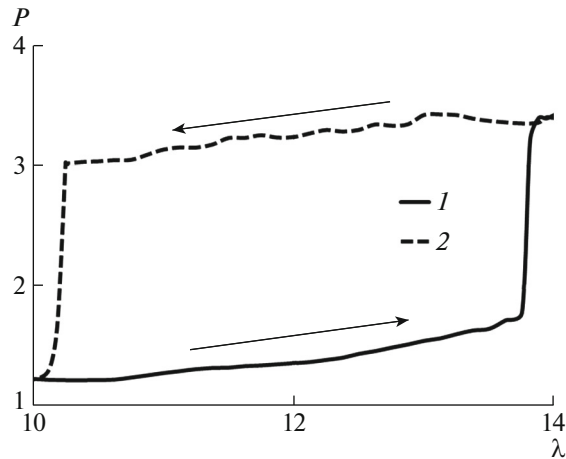


Fig. 3. Changing pressure on the rear ledge of the cavity: (1) depending on an increase, (2) depending on a decrease.

cavity inlet, $\lambda_c = 13-14$. The lower boundary of hysteresis region, λ_o , is more sensitive to changing conditions at the cavity inlet and can vary over a wide range of $\lambda_o = 7-11$. The value of λ_o is determined by the total length of the separation zones behind the anterior and in front of the rear ledges, taking into account the correction for the length of the influence region behind the anterior separation zone [8, 10].

In the case of a supersonic flow over an axisymmetric body with an annular cavity at an angle of attack, the flow conditions exhibit a significant change. The presence of a nonzero angle of attack violates the axial symmetry and leads to an increase in pressure on the windward side of the body surface, as well as the appearance more complicated flow structures.

3. EXPERIMENTAL MODEL AND EXPERIMENTAL CONDITIONS

The following two experimental models were used. One model was used for drainage testing, the other model, for weight testing. Each of them includes a cylindrical body with a diameter of $d = 45$ mm, equipped with a cylindrical head cap and cylindrical tail cap having a diameter of $D = 64$ mm, see Fig. 4. The cavity formed by these bodies in the axial section represents a rectangular cutout with equal heights of the frontal and rear ledges, $h = 9.5$ mm and $h/D = 0.15$. The half-angle of the opening of the conical part of the head nozzle is $\beta = 20^\circ$, conical part length $L_1 = 88$ mm, and length for the cylindrical part of the head cap $L_2 = 14$ mm. The tail cap has length $L_3 = 80$ mm, it can be moved along the axis of symmetry so that relative cavity length $\lambda = L/h$ can be varied in the range of $\lambda = 6-18$.

In the course of weight testing, a model with fixed length $B = 304$ mm was used. Cavity length L in this case was varied via installing additional annular inserts on the body in front of the stern cap with an outer diameter amounting to the diameter of the stern cap.

The experiments were carried out using an A-8 wind tunnel of the Scientific Research Institute of Mechanics, Moscow State University [24] at $M = 2.5$. Air with a stagnation temperature of 270–280 K was used as the working medium. In the case of weight testing, the total pressure in the prechamber amounted to 3.4×10^5 Pa ($Re_1 = 3.5 \times 10^7 \text{ m}^{-1}$). In the case of drainage testing, the total pressure was varied in the range of $(3.4-4.1) \times 10^5$ Pa. The average value of the Mach number in the working part of the wind tunnel calculated based on the results of total and static pressure measurement amounted to $M = 2.54$.

In the course of the experiments, DVR shadow images for flow patterns was carried out. In order to visualize the flow structure, an IAB-451 standard shadow device was used. In order to measure the total aerodynamic forces and moments affecting the model, standard electromechanical four-component scales designed by TsAGI were used. The doser of the alpha mechanism of these scales makes it possible to perform an automatic stepwise change in the angle of attack at an accuracy better than 0.5° . The measurement accuracy in the experiments amounted to 1%, 2%, and 4% for such channels as “drag,” “lift force,” and “pitch moment,” respectively. In the course of the experiment the pressure in the cavity was

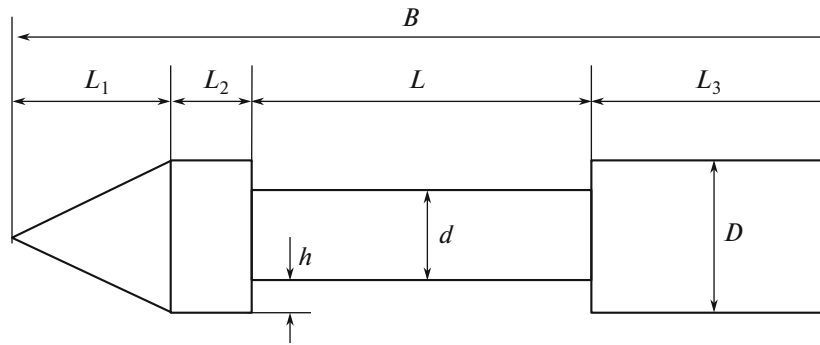


Fig. 4. A schematic diagram of the experimental model.

measured. The measurement points were arranged according to a cross-like pattern on the wall of the rear cavity ledge at a height amounting to $h/2$ from the bottom of the cavity. At that, points X1 and X3 were arranged in the plane of the angle of attack, whereas measurement points X2 and X4 were arranged in the perpendicular plane. Pressure transducers (MR3N6115A type, operating range 15–115 kPa, maximum measurement error ± 1.5 kPa) were located outside the working part of the wind tunnel and were connected to pressure receivers by copper wind tunnels up to 3 m long. The time-averaged static pressure was registered. Owing to the large length of the air path, high-frequency pressure pulsations were smoothed out, and, in fact, a time-averaged static pressure was registered.

In the case of all considered variants, at the moment of wind tunnel launch, the model had a zero angle of attack, $\alpha = 0$. After the wind tunnel entered the operating mode, angle of attack α in the model was changed. First of all, the angle of attack was varied in the range from 0° to -4° , then it was increased to 12° – 16° , and then it was again decreased to 0° . The rate of change in the angle of attack in the experiment amounted to 0.5 deg/s. The measurement error of the current value of α did not exceed $15'$.

4. RESULTS OF VISUALIZATION

In the case of weight testing after the launch of the wind tunnel, only an open flow over the cavity has been observed for all $\lambda < 12$, whereas only a closed one has been registered for all $\lambda \geq 12$. For the case of $\lambda = 12$, when changing the angle of attack, a change in the flow mode has been observed: an initially closed cavity opened, after which it remained open at any subsequent changes in the angle of attack and after the model returning to the initial position. When $\lambda \geq 14$ after the launch of the wind tunnel, a closed pattern appears remaining unchanged in the case of any finite changes in the angle of attack and after a subsequent return of the model to its initial position.

In drainage testing after the launch of the wind tunnel, for all $\lambda < 13.16$, only an open flow over the cavity has been observed, whereas for $\lambda > 13.4$ only a closed one has been registered. At $\lambda = 13.16$, both flow patterns have been observed after launching the wind tunnel, and in a series of five repeated runs of the wind tunnel, an open pattern most often occurs, a closed pattern appears only in one of the five experiments. In the case of appearing closed pattern, at a subsequent change in the angle of attack, an irreversible rearrangement of the flow structure in the cavity towards an open pattern occurs. The open flow pattern has been observed in the case of $\lambda = 13.26$ too.

High-speed video filming has shown that within a period from the moment of wind tunnel launching to the moment when a steady-state flow has established, a chaotic process of changes in a mode of flow over the cavity occurs accompanied by transitions from an open pattern to a closed pattern and vice versa. Significantly higher frequencies occurring in an open flow pattern at $12 \leq \lambda < 13.4$ could indicate a greater stability with respect to external perturbations in the flow mode with an open pattern as to compare to flow modes with a closed pattern in the transition region.

The visualization of flow patterns has shown that in the case of a short cavity ($\lambda < \lambda_0$) at an angle of attack, a combined pattern of flow over the cavity is formed, when a structure with features inherent in a closed pattern is observed on the windward side, whereas a structure characteristic of an open pattern is registered in the case of the leeward side. On the leeward side of a short cavity, the mixing layer separates from the rear ledge of the cavity and propagates almost parallel to the velocity vector of the oncoming flow

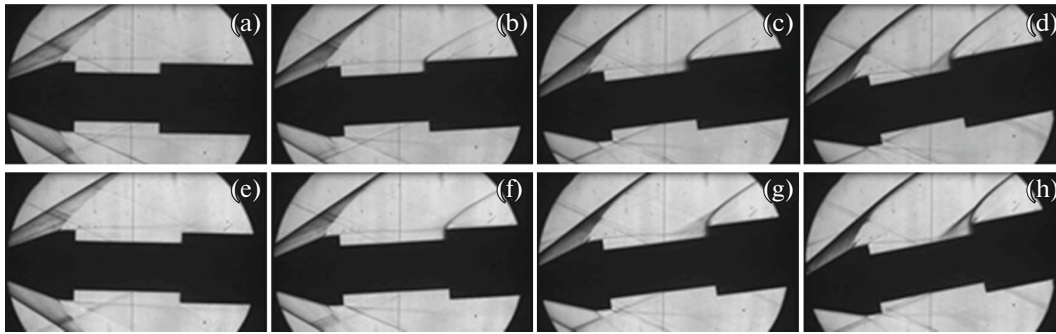


Fig. 5. Visualization of the flow over an open cavity (a–d) for $\lambda = 8$ and (e–h) for $\lambda = 10$ at the following angle of attack: (a, e), (b, f), (c, g), and (d, h) $\alpha = 0^\circ, 4^\circ, 8^\circ,$ and 12° , respectively.

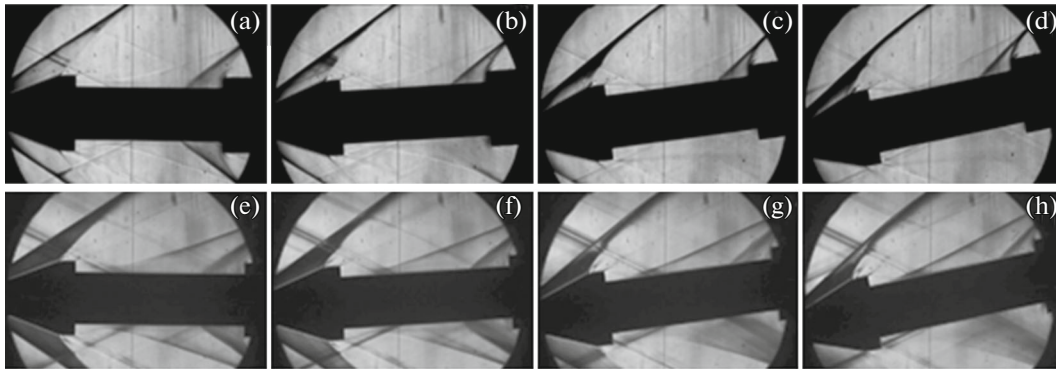


Fig. 6. Visualization of the flow over a closed cavity (a–d) for $\lambda = 14$ and (e–h) for $\lambda = 16$ at the following angle of attack: (a, e), (b, f), (c, g), and (d, h) $\alpha = 0^\circ, 4^\circ, 8^\circ,$ and 12° , respectively.

(see Fig. 5). On the windward side of a short cavity, the mixing layer is pressed against the bottom of the cavity, and as the angle of attack increases in front of the rear ledge, a structure is formed that is characteristic of a closed flow pattern, (Figs. 5b–5d, 5f–5h).

In the case of a long cavity ($\lambda > \lambda_C$), the closed flow pattern remains on the windward side (see Fig. 6). At $\lambda = 14$, with an increase in the angle of attack, a combined pattern occurs, when on the leeward side a transition from a closed pattern (Figs. 6a and 6b) to an open pattern occurs (Figs. 5c and 5d). The rearrangement of the flow structure on the leeward side occurs when a certain critical angle ($\alpha = 5.5^\circ$) is reached. At the same time, on the windward side, an increase in the length of the separation zone behind the front ledge and a shift of the hanging shock-wave tail downstream is observed. The reverse transition from the combined pattern to the closed pattern occurs at lower angles of attack ($\alpha = 5.0^\circ$), i.e., there is a small zone of hysteresis in the angle of attack.

In the case of a more extended cavity ($\lambda \geq 16$), no rearrangement of the flow structure on the leeward side has been observed (Figs. 6e–6h). The closed pattern on the windward and leeward sides remained unchanged at all considered angles of attack. At that, with an increase in the angle of attack, a reduction in the length of the separation zones behind the front and in front of the rear ledges occurs on the windward side. At the same time, on the leeward side the length of the corresponding separation zones exhibits an increase, but no closure of the separation zones occurs.

The flow over cavities with elongation λ belonging to interval $\lambda_O - \lambda_C$ at low angles of attack can occur both in an open and in a closed pattern. Depending on this, there are different scenarios of transitions with an increase in the angle of attack. If at $\alpha = 0$ the flow over the cavity occurs in a closed pattern, then any deviations of the model in the range of small angles of attack do not lead to transitions to a different flow pattern (Figs. 7a–7c). However, the slightest excess of the threshold value of $\alpha = \alpha_k$ ($\alpha_k = 3.8$ at $\lambda = 12$) leads to an abrupt rearrangement from a closed flow pattern to an open one (Figs. 7c and 7d). Moreover,

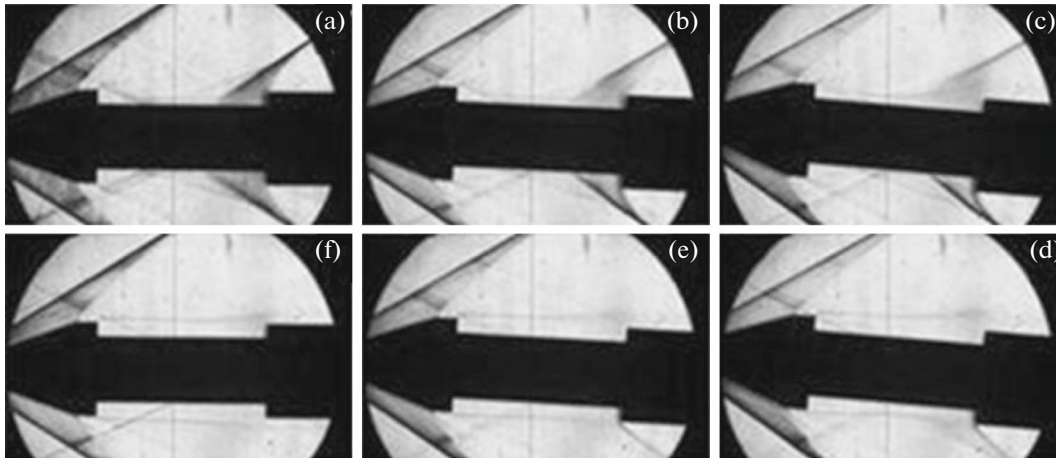


Fig. 7. Structure evolution for the flow over an initially closed cavity in the transition region at $\lambda = 12$ (a–c) in the case of an increase and (d–f) in the case of a subsequent decrease in the angle of attack, as it follows: (a, f), (b, e), and (c, d) $\alpha = 0^\circ, 2^\circ,$ and $3.8^\circ,$ respectively.

this rearrangement is irreversible in the sense that with a subsequent decrease in the angle of attack, the reverse rearrangement no longer occurs (Figs. 7d–7f). On the other hand, if at the initial moment at $\alpha = 0$, the flow over the cavity corresponds to an open pattern, then with an increase in the angle of attack, a transition to a combined flow pattern occurs, whereas with a decrease in the angle of attack, a reverse transition from a combined to an open flow pattern occurs in just the same way. Similar stages in the transition with a change in the angle of attack have been registered for an initially closed pattern at $\alpha = 13.16$ ($\alpha_k = 3.5$). In contrast, at sufficiently close values of $\lambda = 13.44$, the initially closed pattern has proved to be stable with respect to angular perturbations and being restored after any angular displacements of the model in the studied range of angles of attack. At the same time, at $\lambda = 13.26$, an open flow mode is observed. The fact that the existence of an open pattern at $\lambda = 13.26$ occurs and that a relative insensitivity of the closed pattern at $\lambda = 13.44$ with respect to small finite changes in the angle of attack is observed, give grounds to assume that the upper boundary of the transition region lies in the range of $13.26 < \lambda_c < 13.44$. At $\lambda < 12$, only an open cavity was observed; therefore, such an estimate as $\lambda_0 < 12$ is valid for the lower boundary of the transition region.

5. PRESSURE MEASUREMENT RESULTS

The change in pressure on the rear ledge for different types of cavities with a continuous increase/decrease in the angles of attack is illustrated by the graphs presented in Fig. 8.

On the windward side of a short cavity ($\lambda = 8$) with an increase in the angle of attack, the pressure on the rear ledge monotonically increases (Fig. 8a). In the case of a longer open cavity ($\lambda = 13.26$) the situation is qualitatively different (Fig. 8b). In the vicinity of $\alpha = 4^\circ$, an abrupt change in pressure is observed, which could be associated with the above-mentioned rearrangement of the flow structure on the windward side of the cavity towards the transition to a combined flow pattern. With a further increase in the angle of attack, a mode with a closed flow over the windward side of the cavity occurs accompanied by an abrupt increase in pressure on the rear ledge (see graphs for drainage points X1–X4). From this, one can clearly see a hysteresis loop in the angle of attack. In the case of a closed cavity ($\lambda = 14$), the rearrangement of the flow structure occurs on the leeward side. With an increase in the angle of attack, an open pattern appears, whereas with a subsequent decrease in this parameter, a reverse transition to a closed pattern is observed. At the same time, the cavity on the windward side remains closed throughout the entire range of changes in the angle of attack. The graphs plotted for pressure changes on the windward side (point X1) and on the leeward side (point X3) of the rear ledge depending on the angle of attack have a spasmodic character (Fig. 8c). A small hysteresis region is observed, too. At the same time, the pressure at point X2 and point X4 is not sensitive to the structural rearrangement of the flow in the leeward region. At these points, the pressure monotonically decreases (increases) with an increase (decrease) in the angle of attack.

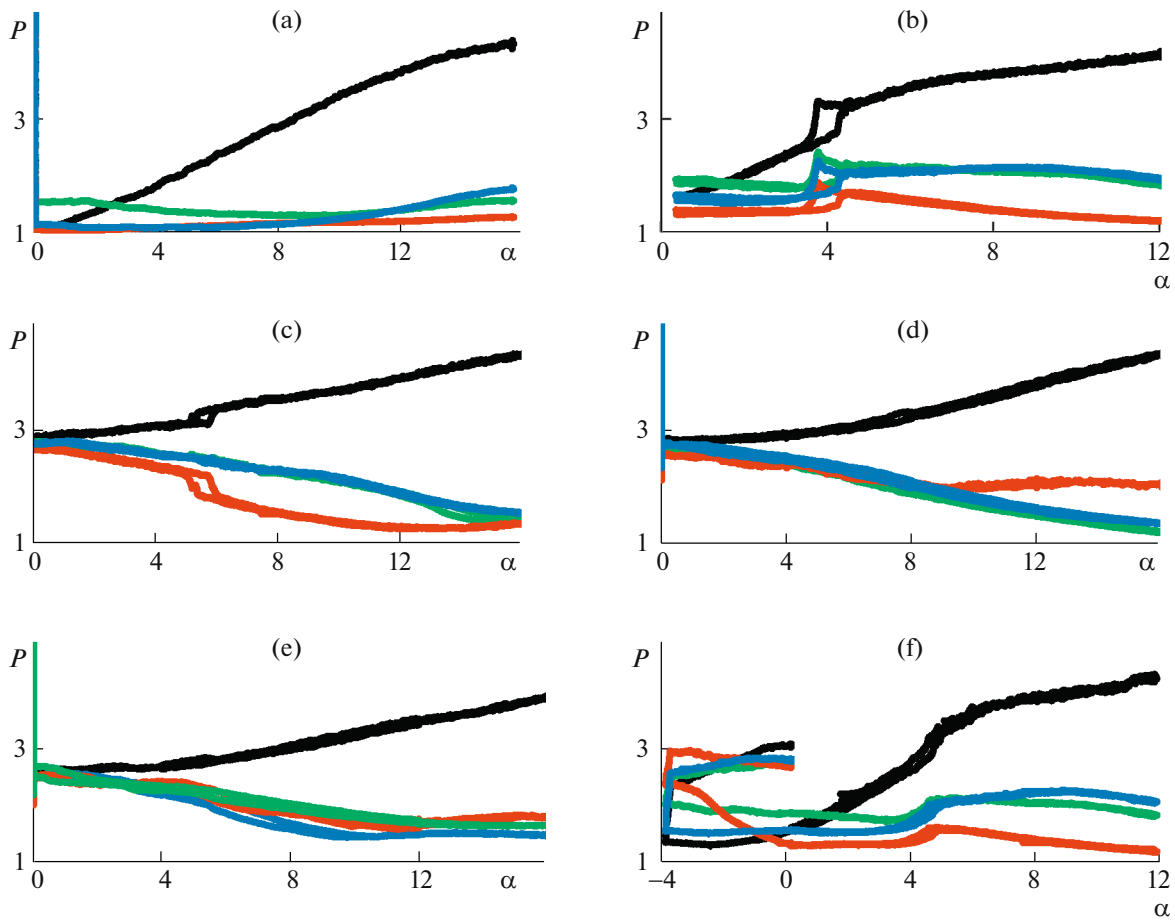


Fig. 8. Changing pressure on the rear ledge ((a, b) $\lambda = 8$ and 13.26) of an open cavity, of a closed cavity ((c–e) $\lambda = 14$, 16 , and 18) and ((f) $\lambda = 13.16$) transitional cavity (black and red line correspond to point X1 and point X3, blue and green line corresponding to point X2 and point X4).

An interesting feature consists in the increase in pressure in the leeward region (point X3) at $\alpha > 12^\circ$. At the same time, at $\alpha = 16^\circ$, the pressure at points X2–X4 almost equalizes.

In the case of a longer cavity ($\lambda = 16$), no structural rearrangement occurs, the closed pattern on the leeward side remains unchanged in the entire considered range of changes in the angle of attack, (see Fig. 6). The pressure at point X1 monotonically increases (decreases) with an increase (decrease) in the angle of attack, whereas at points X2 and X4 the pressure monotonically decreases (increases) with an increase (decrease) in the angle of attack (Fig. 8d). At $\alpha < 8^\circ$, the pressure at point X3 on the rear ledge changes in the same way as it is observed in the case of points X2 and X4, whereas at high angles of attack, the pressure drop in the leeward region (X3) ceases, and the pressure remains almost unchanged for all $\alpha > 8^\circ$. Such pressure behavior at points X2–X4 could be explained by the fact that a localized area with a closed flow structure remains unchanged on the leeward side, whereas in the axial plane passing through points X2 and X4, the closed flow pattern is transformed into an open flow pattern and vice versa, just as it is observed in the case of $\lambda = 14$.

At $\lambda = 18$, the character of pressure changes on the windward (X1) and leeward (X3) sides of the rear ledge remains unchanged. At the same time, the change in pressure at points X2 and X4 is qualitatively and quantitatively similar to the change in pressure at point X3. When $\alpha > 10^\circ$, the pressure at points X2, X3, and X4 exhibits a slight change (Fig. 8e). Apparently, such a character of pressure change at points X2 and X4 is associated with the expansion of the influence of the high-pressure region, which is realized on the leeward side in front of the back ledge of the cavity. The curves obtained for the case of a continuous increase and decrease in the angle of attack for $\lambda = 16$ and 18 almost coincide with each other, which indicates the absence of hysteresis in the angle of attack.

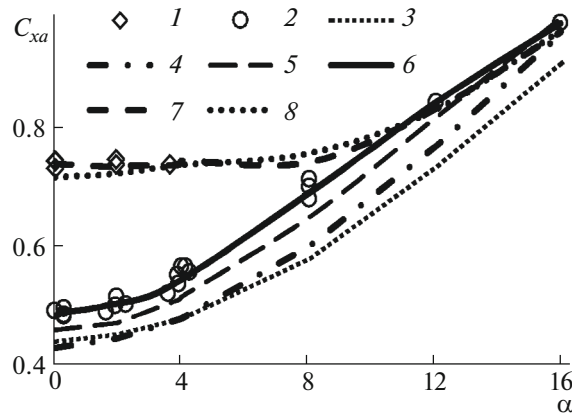


Fig. 9. Effect of the angle of attack on the drag coefficient of the model: (1, 2) $\lambda = 12$; (3–8) $\lambda = 6, 8, 10, 12, 14$, and 16.

Pressure changing in the initially closed cavity in the transition region occurs in a more complicated manner (see Fig. 8f). In the experiment, the angle of attack, at first, has been varied from 0 to -4° , then this parameter increased to 12° , after which it decreased to 0° . The initially closed cavity has opened at an angle of attack amounting to -3.8° , while the pressure at points X1–X4 has abruptly decreased. With a subsequent increase in the angle of attack to the maximum value and then a decrease in the angle of attack to the initial value, the pressure changes just as it is in the case of an open flow pattern, and a transition to the combined flow pattern and back occurs, while no hysteresis in the angle of attack is observed.

Based on the visualization patterns for the flow over the cavity and the data on pressure measurement on the rear ledge, it can be concluded that the rearrangement of the flow structure from an open or closed flow pattern to a combined flow pattern and back is characterized by the presence of a small hysteresis region in an angle of attack for the cavities whose length does not differ much from λ_c .

6. RESULTS OF WEIGHT TESTING

Based on the results of weight testing, drag coefficients C_{xa} , lift force C_{ya} and pitching moment m_z with respect to the model have been determined.

The effect of the angle of attack exerted on the drag coefficient of the model is illustrated by Fig. 9. Curves 3–6 ($\lambda = 6, 8, 10, 12$) have been obtained for flow modes corresponding to an open cavity (at low angles of attack) with a transition to a combined flow pattern at large α . Curves 7 and 8 ($\lambda = 14$ and 16) have been obtained for flow modes corresponding to a closed cavity (at low angles of attack) with a transition to a combined flow pattern at large α . With an increase in the angle of attack, the differences in C_{xa} values are leveled out, so that for $\lambda \geq 8$ at $\alpha = 16^\circ$, the difference in C_{xa} does not exceed 3%. However, there is a tendency to decrease C_{xa} with decreasing λ .

Anomalous C_{xa} behavior is observed in the case of cavities with λ values inherent in the in-length hysteresis region. A corresponding example is shown in Fig. 9, curve 6 ($\lambda = 12$) and data 1–2. In the range of angles of attack $|\alpha| < 3.8^\circ$, dependence C_{xa} on α is ambiguous; in this range of α , there can be modes with open and closed flow patterns. In the case of a closed pattern, an upper branch (1) is observed, whereas in the case of an open pattern a lower branch (2) is registered. At the end of this interval, the closed flow pattern abruptly changes to an open pattern, with an abrupt decrease in the drag coefficient. This transition is irreversible, the further change in the value of the drag coefficient with an increase or decrease in the angle of attack occurs only along curve 6, and in the case of returning to a zero angle of attack, the value of C_{xa} is minimal.

Lift force coefficient C_{ya} and pitching moment coefficient m_z involved in the model are less sensitive with respect to the structural rearrangement of the flow within the cavity. There is a tendency to a decrease in the lifting force with increasing closed cavity length ($\lambda = 14$ and 16), whereas within an open cavity the corresponding force is almost independent of λ (see Fig. 10a). The character of changes in the pitching moment coefficient with respect to the model (Fig. 10b) is consistent with the character of changes in the lift force coefficient. With increasing λ inherent in a closed cavity, a decrease of m_z occurs (in absolute

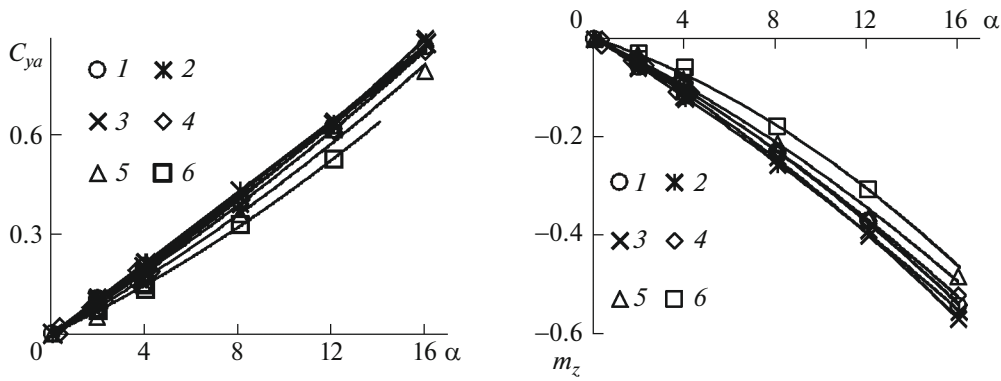


Fig. 10. Effect of the angle of attack (a) on the lift force coefficient and (b) on the pitching moment coefficient: (1–6) $\lambda = 6, 8, 10, 12, 14,$ and 16 .

value). The decrease in $|m_z|$ indicates a decrease in the restoring moment when the model deviates to the final angle of attack. In the case of an open cavity $|m_z|$ almost does not depend on λ .

At small angles of attack, a large scatter in the measurement of forces and moments takes place. On the one hand, this can be caused by the error of model positioning at an angle of attack amounting up to 0.25° in absolute value. The data scatter at $\lambda = 12$ can be also associated with the ambiguity of the flow structure in the cavity at angles of attack less than 4° , which is reflected by the graph plotted for changing the drag force (see Fig. 9).

7. CONCLUSIONS

Based on flow visualization, pressure measurements and weight testing for relative cavity length ranging from 6 to 18 at a continuous change in the angle of attack ranging from -4° to 16° , an evolution of the structure and parameters of the flow over an annular cavity at Mach number $M = 2.5$ has been studied. A hysteresis range in the cavity length, where flow structures with closed and open flow patterns can coexist at low angles of attack has been identified. The flow’s structural rearrangement from a closed pattern to an open pattern occurs irreversibly with an increase in the angle of attack and is accompanied with an abrupt decrease in the cavity drag.

At high angles of attack, a transition to a combined flow pattern occurs having the features of a closed pattern on the windward side of the cavity and those of an open pattern on the leeward side. The structural rearrangement of the flow to a combined pattern of flow over an annular cavity and vice versa is characterized by a small hysteresis region in the angle of attack. There is a tendency for the lift force to decrease with increasing closed cavity length, whereas in an open cavity the corresponding force is almost independent of λ . The character of change in the pitching moment coefficient is consistent with the character of change in the lift coefficient.

The revealed features of flow over axisymmetric bodies with annular cavities should be taken into account in designing aircraft elements. The results can also serve as a testing example for computational technologies for calculating three-dimensional separated flows. At the same time, a detailed analysis of the structure inherent in the combined mode of flow over an annular cavity revealed in a physical experiment is hardly possible without any computational experiments.

FUNDING

The study was financially supported as part of the State Budget topic AAAA-A16-116021110201-2 for the Scientific Research Institute of Mechanics, Moscow State University (<http://www.imec.msu.ru>).

REFERENCES

1. Charwat, A.F., Roos, J.N., Dewey, F.C., and Hitz, J.A., An investigation of separated flows-part i: the pressure field, *J. Aerospace Sci.*, 1961, vol. 28, pp. 457–470.

2. Stalling, R.L. and Wilcox, F.J., Experimental cavity pressure distribution at supersonic speeds, *NASA Tech. Pap.*, 1987, no. 2683.
3. Zhang, J., Morishita, E., Okunuki, T., and Itoh, H., Experimental investigation on the mechanism of flow-type changes in supersonic cavity flows, *Trans. Jpn. Soc. Aeron. Space Sci.*, 2002, vol. 45, no. 149, pp. 170–179.
4. Lawson, S.J. and Barakos, G.N., Review of numerical simulations for high-speed, turbulent cavity flows, *Progr. Aerospace Sci.*, 2011, vol. 47, pp. 186–216.
5. Chang, P.K., *Separation of Flow*, Pergamon Press, 1970, vol. 2.
6. Penzun, V.I., Separation flow in circular cavity, *Uch. Zap. TsAGI*, 1976, vol. 6, pp. 124–130.
7. Shvets, A.I., Investigation of the flow in an annular cavity in a cylindrical body in a supersonic stream, *Fluid Dyn.*, 2002, vol. 37, no. 1, pp. 109–116.
8. Guvernuyuk, S.V., Zubkov, A.F., and Simonenko, M.M., Aerodynamical hysteresis under supersonic flow-round the circular cavity at axisymmetric body, in *Uspekhi mekhaniki sploshnykh sred. Sb. dokladov Mezhdunarodnoi konferentsii, priurochennoi k 75-letiyu akad. V.A. Levina* (Proc. Int. Conf. Dedicated to 75th Anniversary of V.A. Levin, Academician), Irkutsk: OOO “Megaprint,” 2014, pp. 163–168.
9. Guvernuyuk, S.V., Zubkov, A.F., Simonenko, M.M., and Shvets, A.I., Experimental investigation of three-dimensional supersonic flow past an axisymmetric body with an annular cavity, *Fluid Dyn.*, 2014, vol. 49, no. 4, pp. 540–547.
10. Guvernuyuk, S.V., Zubkov, A.F., and Simonenko, M.M., Experimental investigation of the supersonic flow over an axisymmetric annular cavity, *J. Eng. Phys. and Thermophys.*, 2016, vol. 89, no. 3, pp. 678–687.
11. Mohri, K. and Hillier, R., Computational and experimental study of supersonic flow over axisymmetric cavities, *Shock Waves*, 2011, vol. 21, pp. 175–191.
12. Sinha, J., Das, S., Kumar, P., and Prasad, J.K., Computational investigation of control effectiveness on a near transition open and closed axisymmetric cavity, *Adv. Aerospace Sci. Appl.*, 2014, vol. 4, no. 1, pp. 45–52.
13. Savel'ev, A.D., Numerical simulation of longitudinal cavities flow-round by supersonic flow, *Uch. Zap. TsAGI*, 2011, vol. 42, no. 3, pp. 60–72.
14. Aksenov, A.A., Guvernuyuk, S.V., Deryugin, Yu.N., et al., Numerical research on hysteresis of supersonic turbulent flow for a body with circular cavity by means of Logos software complex, in *Materialy 14-oi Mezhdunar. konf. "Supervychisleniya i matematicheskoe modelirovanie"* (Proc. 14th Int. Conf. “Supercalculations and Mathematical Simulation”), Sarov: Russian Federal Nuclear Center All-Russian Research Institute of Experimental Physics, 2012, pp. 164–166.
15. Ivanov, I.E., Kryukov, I.A., Larina, E.V., and Tarasevich, A.G., Numerical simulation of flow over axisymmetric body with annular cavity, *Fiz.-Khim. Kinet. Gaz. Din.*, 2015, vol. 16, no. 2.
<http://chemphys.edu.ru/issues/2015-16-2/articles/583/>.
16. Zhang, X. and Edwardst, J.A., Experimental investigation of supersonic flow over two cavities in tandem, *AIAA J.*, 1992, vol. 30, no. 5, pp. 1182–1190.
17. Zaikovskii, V.N., Smul'skii, Ya.I., and Trofimov, V.M., Sequential cavities effect onto heat exchange in supersonic flow, *Teplofiz. Aeromekh.*, 2002, vol. 3, pp. 423–430.
18. Palharini, R.C. and Scanlon, T.J., Aerothermodynamic comparison of two- and three-dimensional rarefied hypersonic cavity flows, *J. Spacecraft Rockets*, 2014, vol. 51, no. 5, pp. 1691–1630.
19. Cattafesta, L.N., Song, Q., Williams, D.R., Rowley, C.W., and Alvi, F.S., Active control of flow-induced cavity oscillations, *Progr. Aerospace Sci.*, 2008, vol. 44, pp. 479–502.
20. Zhuang, N., Alvi, F.S., Alkisar, M.B., and Shih, C., Supersonic cavity flows and their control, *AIAA J.*, 2006, vol. 44, no. 9, pp. 2118–2128.
21. Vikramaditya, N.S. and Kurian, J., Experimental study of influence of trailing wall geometry on cavity oscillations in supersonic flow, *Exp. Therm. Fluid Sci.*, 2014, vol. 54, pp. 102–109.
22. Mathur, T., Gruber, M., Jackson, K., Donbar, J., Donaldson, W., Jackson, T., and Billig, F., Supersonic combustion experiments with a cavity-based fuel injector, *J. Propul. Power*, 2001, vol. 17, no. 6, pp. 1305–1312.
23. Ukai, T., Zare-Behtash, H., Erdem, E., Lo, K.H., Kontis, K., and Obayashi, S., Effectiveness of jet location on mixing characteristics inside a cavity in supersonic flow, *Exp. Therm. Fluid Sci.*, 2014, vol. 52, pp. 59–67.
24. *Aerodinamicheskie ustanovki Instituta mekhaniki Moskovskogo universiteta* (Aerodynamical Plants in Mechanical Institute of Moscow State University), Chernii, G.G., Zubkov, A.I., and Panov, Yu.A., Eds., Moscow: MSU, 1985.

Translated by O. Polyakov